NJC

Accepted Manuscript

This is an *Accepted Manuscript*, which has been through the Royal Society of Chemistry peer review process and has been accepted for publication.

Accepted Manuscripts are published online shortly after acceptance, before technical editing, formatting and proof reading. Using this free service, authors can make their results available to the community, in citable form, before we publish the edited article. We will replace this *Accepted Manuscript* with the edited and formatted *Advance Article* as soon as it is available.

You can find more information about *Accepted Manuscripts* in the Information for Authors.

Please note that technical editing may introduce minor changes to the text and/or graphics, which may alter content. The journal's standard Terms & Conditions and the Ethical guidelines still apply. In no event shall the Royal Society of Chemistry be held responsible for any errors or omissions in this *Accepted Manuscript* or any consequences arising from the use of any information it contains.

ROYAL SOCIETY OF CHEMISTRY

www.rsc.org/njc

Optical and theoretical studies on Fe_3O_4 - imidazole nano composite and clusters

Jayaraman Jayabharathi*, Periyasamy Ramanathan, Venugopal Thanikachalam, Chockalingam Karunakaran

Department of Chemistry, Annamalai University, Annamalainagar 608 002, Tamilnadu, India.

* Address for correspondence
Dr. J. Jayabharathi
Professor of Chemistry
Department of Chemistry
Annamalai University
Annamalainagar 608 002
Tamilnadu, India.
Tel: +91 9443940735
E-mail: jtchalam2005@yahoo.co.in

* Corresponding author. Tel.: +91 9443940735
E-mail address: jtchalam2005@yahoo.co.in

Optical and theoretical studies on Fe_3O_4 - imidazole nano composite and clusters

Jayaraman Jayabharathi*, Periyasamy Ramanathan, Venugopal Thanikachalam, Chockalingam Karunakaran

Department of Chemistry, Annamalai University, Annamalainagar 608 002, Tamilnadu, India.

Abstract

N,N-dimethyl-4-(1-phenyl-1H-phenanthro[9,10-d]imidazol-2-yl)naphthalen-1-amine (DMPPINA) has been synthesised using sol-gel prepared TiO_2 rutile as catalyst under solvent free condition and characterized by NMR spectral studies. The synthesised phenanthrimidazole bound magnetic nanoparticles (Fe_3O_4-DMPPINA composite) have been characterized using scanning electron microscopy (SEM), transmission electron microscopy (TEM), energy dispersive X-ray spectroscopy (EDS), X-ray diffractometry (XRD) and lifetime and Fourier-transform infrared spectroscopies (FT-IR). The intensities of absorption and emission of the Fe_3O_4-DMPPINA composite is higher than DMPPINA. Conductance and VSM measurements were also carried out. The prototropic study of DMPPINA has been made to show the increase of electron density at azomethine nitrogen atom due to charge transfer from N,N-dimethylamino group to azomethine nitrogen atom. The molecular electrostatic potential surface (MEP) has also been employed to show the higher electron density at azomethine nitrogen atom. Theoretical investigation shows that the calculated binding energy and energy gap of the imidazole composite are highly dependent on the nature of the iron oxide cluster. We have studied in detail the site-specific binding nature and the adsorption strength of imidazole with different iron oxide clusters.

Keywords: TiO_2 (R); Fe_3O_4-DMPPINA composite; FT-IR; SEM; TEM; EDS; XRD

* Corresponding author. Tel.: +91 9443940735
E-mail address: jtchalam2005@yahoo.co.in

1. Introduction

Arylimidazoles play important role in materials science and medicinal chemistry due to their optoelectronic properties and high thermal stabilities [1-6]. Substituted imidazoles are extensively used as glucagon receptors [7], antibacterial [8], anti-allergic [9], analgesic [10] and antitumor [11] agents and also as pesticides [12]. Since many of the reported synthetic protocols for imidazoles [13-24] suffer from disadvantages development of a new catalyst is of interest. From the synthetic point of view, titanium dioxide [25] has been used as a potential green, inexpensive, mild and recyclable heterogeneous Lewis acid catalyst in organic transformations including synthesis of phenanthrimidazole [26].

Among the magnetic nanoparticles, Fe_3O_4 nanoparticles are of current interest because of their unique magnetic properties [27]. Magnetic nanoparticle aggregates were formed using polyethylene glycol nonylphenyl ether and cyclodextrin in aqueous medium [28] and Fe_3O_4 colloidal nanocrystal clusters were created by high-temperature hydrolysis reaction [29]. Fe_3O_4–polyaniline nanocomposites were formed by chemical oxidation polymerization [30]. The nanoparticles of iron oxides have been extensively exploited as materials of choice for ferrofluids, high-density information storage, magnetic resonance imaging (MRI), drug delivery, labelling, etc., [31]. The development of biocompatible nano sized drug delivery systems such as magnetic iron oxide nanoparticles, for specific targeting of therapeutics is the focus of medical research. An important advantage of nano iron oxide carriers is the possibility for detecting these nanoparticles after treatment with common imaging techniques like x-ray-tomography, magnetorelaxometry and MRI [31].

The optoelectronic studies of nano Fe_3O_4 with some ligands such as polyacrylic acid, oleic acid, n-octadecyltrichlorosilane, polyaniline, poly (N-vinyl-2-pyrrolidine), etc., have been reported [32]. However, such study with imidazole is lacking and this study addresses the same. Here we report a simple one-pot synthesis of phenanthrimidazole in good yield using

sol-gel synthesised nano titanium dioxide under solvent free condition. More importantly, we focus on the synthesis of cubic Fe_3O_4 and Fe_3O_4–DMPPINA nanocomposites, characterizing them by XRD, SEM, TEM, VSM, etc., and the optical, electrical and magnetic properties of DMPPINA, Fe_3O_4 and Fe_3O_4 – DMPPINA composite. Drug molecules invariably contain nitrogen and the activity of drug depends on the electron density at nitrogen. pH of the medium alters the electron density at nitrogen and hence it is thought worthwhile to probe the prototropic mechanism of DMPPINA also; Fe_3O_4-DMPPINA composite are unlikely to be stable in acedic pH and hence theoretical investigation has been carried out to understand the strength of binding interaction of DMPPINA with different iron oxide clusters.

2. Experimental

2.1. Materials and measurements

Titanium(IV) isopropoxide, ferric nitrate, ethylene glycol, dimethyl sulphoxide, isopropyl alcohol, ammonium acetate, ethyl acetate, benzene, phenanthriquinone, aniline, 4-(dimethylamino)-1-naphthaldehyde and all other reagents have been purchased from Sigma-aldrich. NMR spectra were recorded on Bruker 400 MHz NMR spectrometer and the mass spectra were obtained using an Agilent LCMS VL SD in electron ionization mode. The UV-vis and photoluminescence spectra were recorded with Perkin Elmer Lambda 35 UV-vis spectrophotometer and PerkinElmer LS55 fluorescence spectrometer, respectively. Cyclic voltammetry (CV) analysis were performed by using CHI 630A potentiostat electrochemical analyzer. Measurements of oxidation and reduction were undertaken using 0.1M tetra(n-butyl)ammonium- hexafluorophosphate as the supporting electrolyte, at scan rate of $0.1VS^{-1}$. The potentials were measured against an Ag/Ag^+ (0.01M $AgNO_3$) reference electrode using quinine sulphate as the internal standard. The onset potentials were determined from the intersection of two tangents drawn at the rising current and background current of the cyclic voltammogram. Fluorescence lifetime measurements were carried out with CHI 630A

potentiostat electrochemical analyzer and Horiba Fluorocube-01-NL lifetime system with nano LED as the excitation source and TBX-PS as detector, respectively. The quantum yields were measured by comparing fluorescence intensities of a standard sample [anthracene; Φ_{std} = 27%; η_{std} = 1.36] [33a] and theoretical calculations were performed using Gaussian-03 program [33b]. Vibrating sample magnetometer (Oxford, VSM) was used to evaluate magnetic moments of the prepared nanocomposites as a function of the applied magnetic field 10 or 15 kOe at room temperature. TEM analysis was carried out using JEOL JEM 2100 high resolution transmission electron microscope (HR-TEM) with an accelerating voltage of 200 kV. The samples were dispersed in acetone and spread on the grid for imaging. Formavar coated copper grids were used for loading the sample. XRD patterns were recorded for the centrifuged and dried samples using X–ray Rigaku diffractometer with Cu K_α source (30 kV, 100 mA), at a scan speed of 3.0000 deg/min, step width of 0.1000 deg, in a 2θ range of 20-80°. The energy dispersive X-ray spectra were recorded with a JEOL JSM-5610 scanning electron microscope equipped with back electron (BE) detector and EDX. The sample was placed on an adhesive carbon slice supported on copper stubs and coated with 10 nm thick gold using JEOL JFC- 1600 auto fine coater prior to measurement.

2.2.Molecular Electrostatic Potential (MEP) calculation

In the present work MEPs derive from a classical point charge model. The electrostatic potential for each molecule is obtained by moving a unit positive point charge across the van der Waals surface and it is calculated at various points *j* on this surface using, $V_j = q_i / r_{ji}$ where q_i represents the partial charge of each atom *i* and r_{ji} is the distance between point's *j* and atom *i*. Starting from the 3D model of a molecule and its partial atomic charges, the electrostatic potential is calculated for points on the molecular surface.

2.3. Synthezis of N,N-dimethyl-4-(1-phenyl-1H-phenanthro[9,10-d]imidazol-2-yl)naphthalen-1-amine (DMPPINA)

A mixture of 4-(dimethylamino)-1-naphthaldehyde (1 mmol), phenanthrene-9,10-dione (1 mmol), aniline (1 mmol) and ammonium acetate (1 mmol) with TiO_2 (1 mol%) as catalyst was stirred at 120 °C with continuous stirring with a bar magnet. The progress of the reaction was monitored by TLC (Scheme S1). After completion of the reaction, 10 ml of ethyl acetate was added to the reaction mixture and shaken well to dissolve the organic components and the mass filtered to separate out TiO_2 and the residue was washed with ethyl acetate. The solid residue of TiO_2 was further washed with hot acetone and then dried up. The product was purified by column chromatography using benzene: ethyl acetate (9:1) as the eluent. The newly synthesised phenanthrimidazole has been characterised by ^1H and ^{13}C NMR and mass (MS) spectra. Yield: 75%, M.p. 258 ºC., Anal. calcd. for $C_{33}H_{25}N_3$: C, 85.50; H, 5.44; N, 9.06. Found: C, 85.49; H, 5.43; N, 9.05. ^1H NMR (400 MHz, DMSO): δ 3.46 (s, 6H), 9.23 (d, J = 8.4 Hz, 1H), 8.87 (s, 2H), 8.69 (s, 1H), 8.61 (s, 1H), 8.16 (d, J = 7.2 Hz, 1H), 8.11 (d, J = 8.0 Hz, 1H), 8.07 (dd, J = 8.0 Hz, 1H), 7.78-7.62 (m, 8H), 7.34 (s, 2H). ^{13}C NMR (400 MHz, DMSO): δ 43.88, 122.02, 122.42, 123.78, 124.03, 124.30, 124.69, 125.28, 126.32, 126.40, 126.88, 127.05, 127.15, 127.63, 127.77, 128.28, 128.38, 128.67, 128.99, 129.08, 129.25, 129.75, 130.61, 131.13, 133.65, 135.21, 135.35, 136.79, 137.02, 149.04, 151.82, 178.94, 189.42, 194.35. MS: m/z. 463 [M+].

2.4. Synthesis of Fe_3O_4 – DMPPINA composite

About 1 mmol of DMPPINA in dimethyl sulphoxide was added to 1 mmol of Fe_3O_4 nanoparticles suspended in dimethyl sulphoxide under constant stirring for 3 h. The solid was filtered, washed with dimethyl sulphoxide and dried at 110 ºC.

3. Results and discussion

3.1. Characterization of nano TiO_2 (R) and the catalysed synthesis

Nanocrystalline rutile TiO_2 obtained by sol–gel method has been characterized by XRD, SEM and energy dispersive X - ray, UV–visible diffuse reflectance (DRS) and solid state

photoluminescence spectroscopies. The crystalline phase, average crystalline size (20.4 nm) and surface area (51.7 m^2/g) have been determined by powder XRD (Figure 1). The SEM image (Figure 1) reveals agglomeration of the synthesized nanoparticles. UV-visible DRS (Figure 2) provides the band gap as 3.19 eV. The observed slightly larger band gap is because of the smaller size of the nanoparticles. Quantum confinement effect increases the band gap energy. The PL spectrum (Figure 2) show emissions at 411, 450, 482 and 530 nm. These emissions are due to trapped electrons and oxygen vacancies [34].

3.2. Catalytic activity of TiO_2 (R) semiconductor

Initially, we have carried out the condensation reaction in the presence of TiO_2(R) (1mol %), 4-(dimethylamino)-1-naphthaldehyde (1 mmol), ammonium acetate (1 mmol) and aniline (1 mmol) in different solvents such as water, ethanol, methanol, chloroform and acetonitrile under refluxing and also in solvent-free condition at 120 °C (Scheme S1). From these experiments, it was clearly demonstrated that the solvent-free condition is the best for phenanthrimidazole synthesis. In the absence of catalyst under solvent-free condition at room temperature the yield is very poor even after 24 hr. To enhance the yield of the desired product, the temperature of the reaction was increased to 180 ºC, but no appreciable increment in the product yield was observed. We found that presence of a catalytic amount of TiO_2(R) under solvent-free condition is the best for this synthesis; maximum yield (82%) was obtained at 30 min on loading with 1mol% of TiO_2 (R) at 120 °C (Table 1). Moreover, TiO_2 can be recovered and reused several times without significant loss of activity (Scheme 1). High product yield, shorter reaction time, low catalyst loading and easy work-up procedure, make this procedure quite simple and more convenient. Our methodology could be a valid contribution to the existing processes of imidazole synthesis.

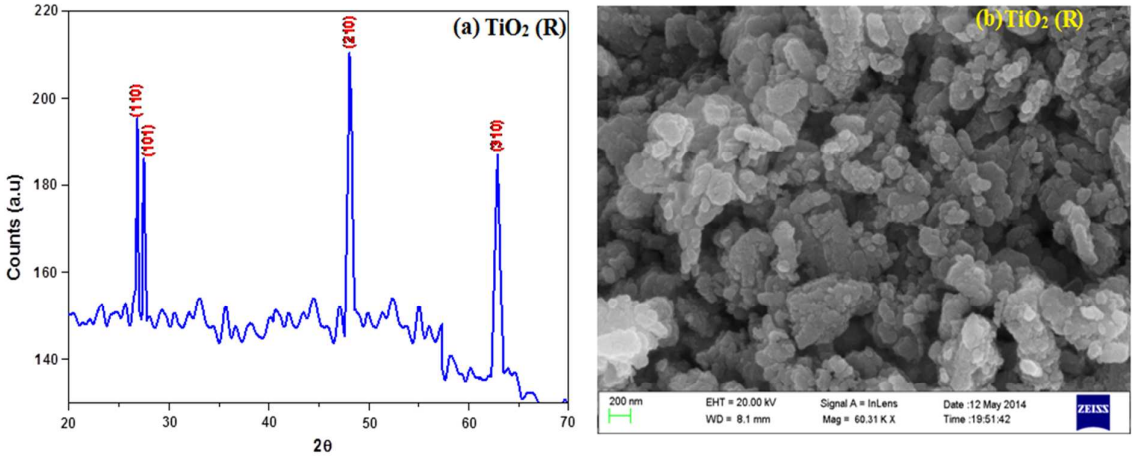

Figure 1. (**a**) X-ray diffraction pattern (XRD) of TiO_2 (R); (**b**) SEM image of TiO_2 (R)

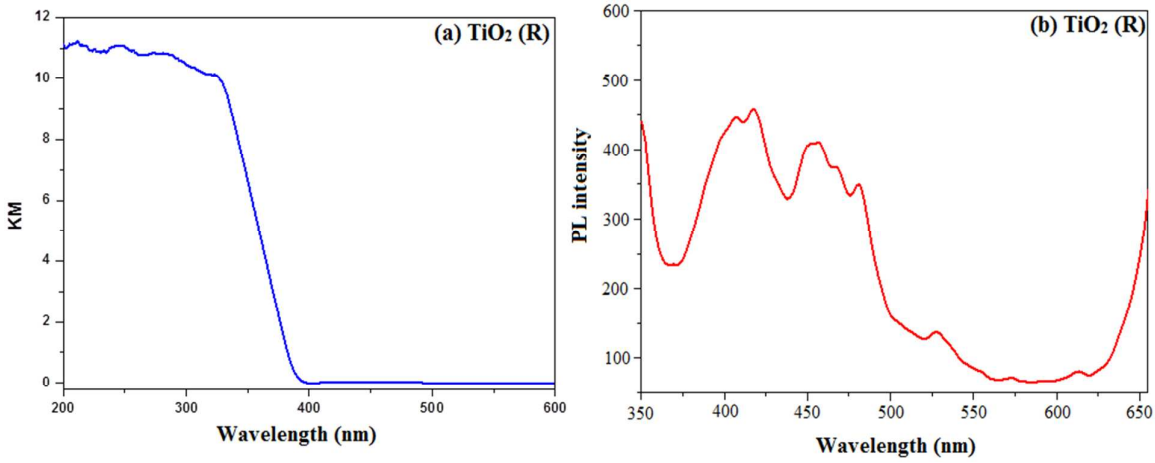

Figure 2. (**a**) Diffused reflectance spectra of TiO_2 (R); (**b**) Solid state photoluminescence spectra of TiO_2 (R)

Table 1. Effect of catalyst and temperature in the synthesis of phenanthrimidazoles

Entry	Temp (°C)	solvent	TiO_2 Time (min)	TiO_2 Yield (%)	TiO_2 (mol%)
1	r.t	Solvent-free	125	60(Trace)	0.1
2	50	Solvent-free	62	65(20)	0.1
3	70	Solvent-free	35	68(45)	0.1
4	90	Solvent-free	20	70(50)	0.1
5	120	Solvent-free	30	75	1
6	120	Solvent-free	25	78	2
7	120	Solvent-free	40	80	10
8	120	Water	100	20	1
9	120	Ethanol	40	40	1
10	120	Methanol	50	45	1
11	120	Chloroform	140	42	1
12	120	Acetonitrile	95	50	1

values in the parenthesis represent without catalyst

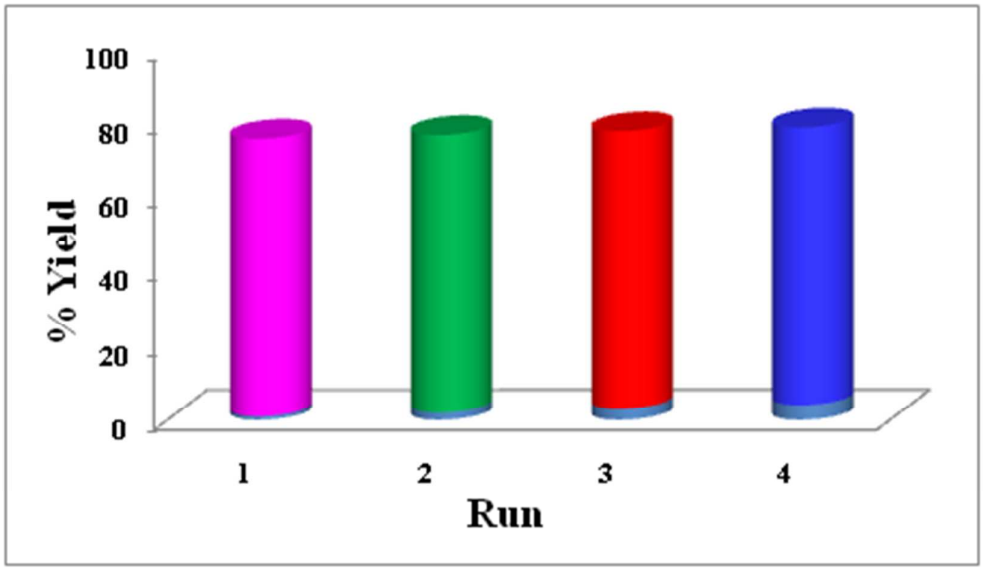

Scheme 1. Reusability of TiO_2 (R) for catalytic synthesis of phenanthrimidazoles

3.3. Structure, morphology, magnetic and electrical properties of Fe_3O_4 – DMPPINA composite

Figure 3 displays the powder diffraction pattern of face centred cubic Fe_3O_4. The recorded XRD of Fe_3O_4 nanoparticles is in agreement with JCPDS No. 19-0629. The diffraction peaks at 24.1, 33.1, 35.6, 49.4, 54.0 62.5 and 64.1° correspond to 111, 220, 311, 400, 422, 440 and 511 planes, respectively. The mean crystallite size (L) of the cubic Fe_3O_4 is 12 nm and the calculated surface area is 96 m^2/g. Figure 3 displays the powder diffraction pattern of Fe_3O_4 – DMPPINA composite. The recorded XRD of Fe_3O_4 – DMPPINA composite is in agreement with JCPDS No. 19-0629. The diffraction peaks at 24.2, 33.3, 35.7, 49.5, 54.2 62.4 and 64.2° correspond to 111, 220, 311, 400, 422, 440 and 511 planes, respectively. The mean crystallite size (L) of the Fe_3O_4 – DMPPINA composite is 12 nm and the calculated surface area is 96 m^2/g. The TEM images of cubic Fe_3O_4 and Fe_3O_4 – DMPPINA composite are shown in figure 3. The TEM images of pristine Fe_3O_4 and Fe_3O_4 – DMPPINA composite confirm that they are nanoparticles and the average measured particles size (pristine - 22 nm, Fe_3O_4 – DMPPINA - 20 nm) is larger than the average crystalline size deduced from the XRD (20 nm) results. This indicates that nanoparticles associates among themselves. Although most of the particles are appear to be of comparable size there are a few which are of larger size. This is so in pristine as well as DMPPINA bound Fe_3O_4 nanocomposites.

The SEM images of cubic Fe_3O_4 and Fe_3O_4 – DMPPINA composite are shown in Figure 4 reveal the agglomeration of the nanoparticles. The EDX spectra of cubic Fe_3O_4 and Fe_3O_4 – DMPPINA composite are shown in Figure 5. They display the presence of carbon and nitrogen along with iron in the composite. This shows the binding of phenanthrimidazole with Fe_3O_4 nanoparticles.

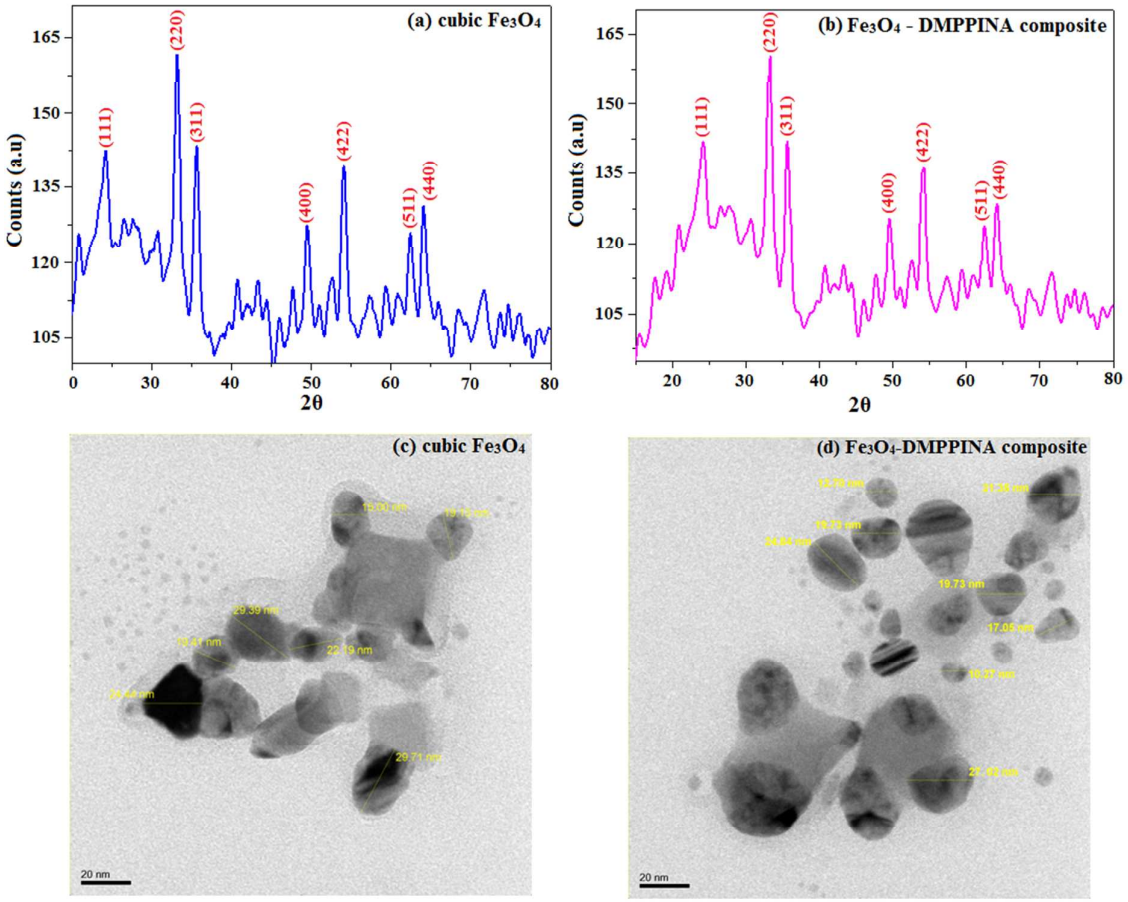

Figure 3. Powder X-ray diffraction (XRD) pattern of (**a**) cubic Fe_3O_4; (**b**) Fe_3O_4-DMPPINA composite; TEM images of (**c**) cubic Fe_3O_4; (**d**) Fe_3O_4-DMPPINA composite

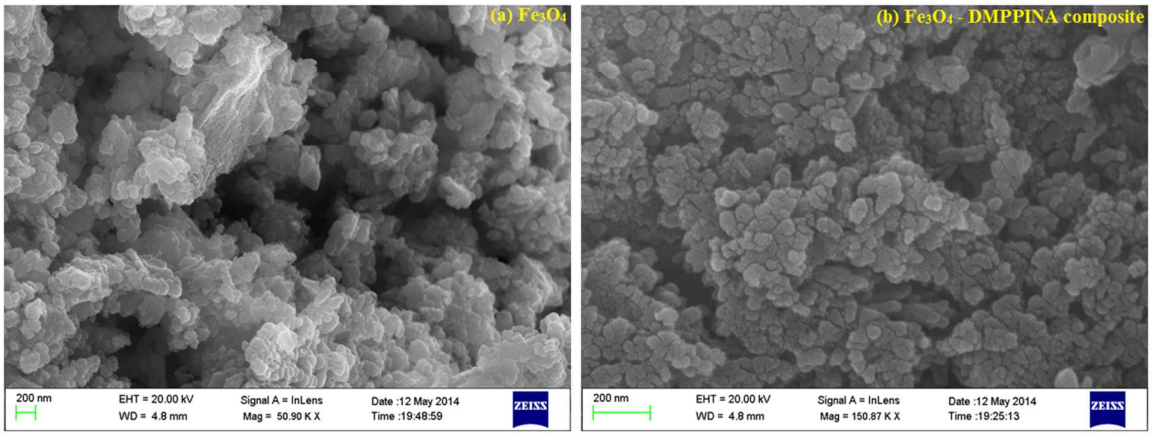

Figure 4. SEM images of (**a**) cubic Fe_3O_4 and (**b**) Fe_3O_4-DMPPINA composite

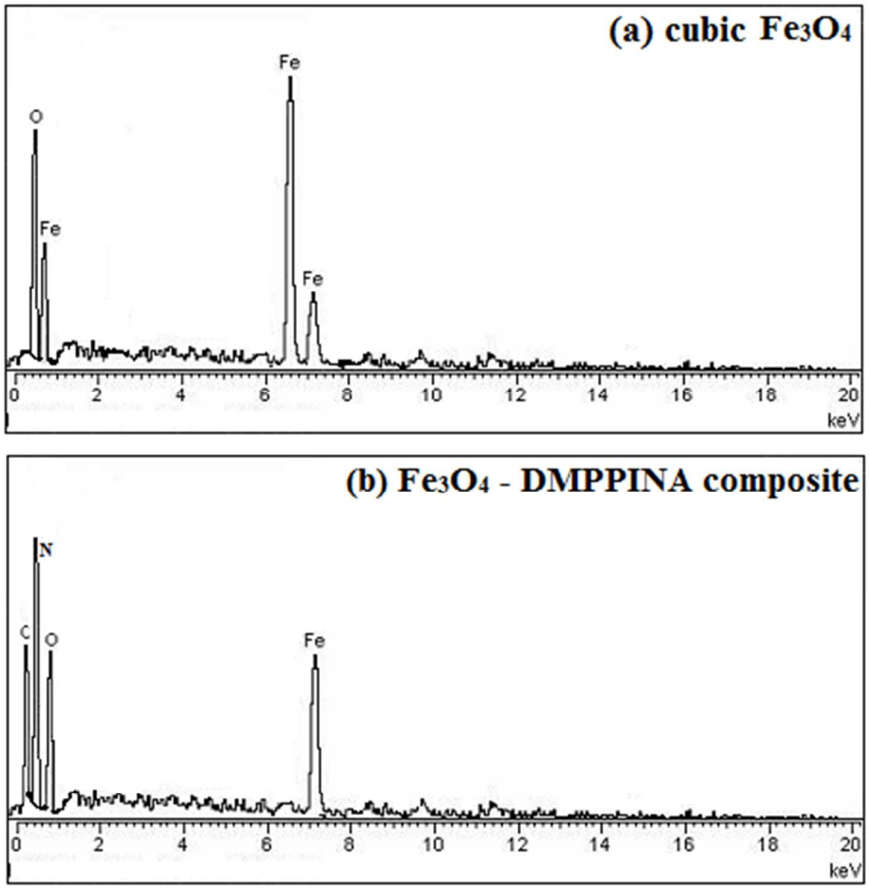

Figure 5. EDX spectra of (**a**) cubic Fe_3O_4 and (**b**) Fe_3O_4-DMPPINA composite

Magnetic hysteresis curves recorded at room temperature for pristine Fe_3O_4 and Fe_3O_4-DMPPINA composite are presented in Figure 6. Magnetic parameters like saturation magnetization (M_S), coercivity (H_C) and remanence magnetization (M_R) have been evaluated. The magnetic measurements show pristine Fe_3O_4 as superparamagnetic nanoparticles. The hysteresis loops exhibit ferromagnetic behavior, with saturation magnetization (M_S) of 1.6 emu g^{-1}, coercivity (H_C) of 35 Oe and remanant magnetization (M_R) of 0.1 emu g^{-1}, respectively. On the other hand the M-S curve of DMPPINA – bound Fe_3O_4 nanoparticles shows steady increase of magnetisation with applied voltage. Further, the significant "thickness" of the loop reflects suppression of the superparamagnetic behaviour on binding DMPPINA with Fe_3O_4 nanoparticles. The saturation magnetisation is also suppressed to about 0.027 emu g^{-1}. The Ms value of Fe_3O_4 nanoparticles is determined by the methods of

synthesis [35] and a possible reason for the observed low M_S value could be crystalline defects and alignment of magnetic moment in nanocrystals.

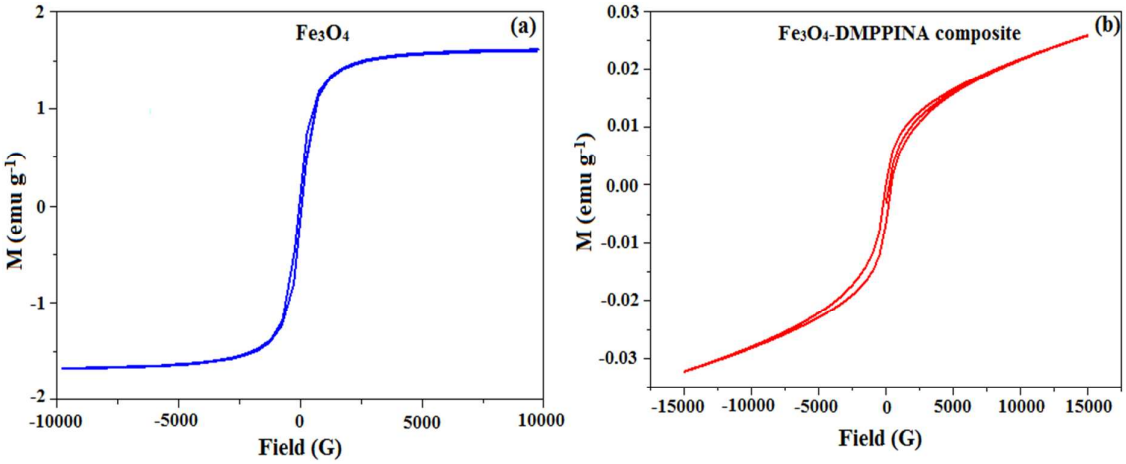

Figure 6. VSM spectra of (**a**) cubic Fe_3O_4; (**b**) Fe_3O_4-DMPPINA composite

The FT-IR spectra of DMPPINA, Fe_3O_4 nanoparticles and Fe_3O_4 – DMPPINA composite, are shown in Figure 7 and the prominent frequencies are displayed in Table 2. The frequency around 1600 cm^{-1} corresponds to C=N function of imidazole and Fe_3O_4-DMPPINA composite. The peak around 3426 cm^{-1} corresponds to ≥ C-H in DMPPINA and Fe_3O_4 – DMPPINA composite. The peak at ~ 745 cm^{-1} is likely due to the aromatic C-H stretching. The frequencies at 1645 and 1633 cm^{-1} are assigned to Fe-O stretching vibration in Fe_3O_4-DMPPINA composite and Fe_3O_4 nanoparticles, respectively. The Fe-O stretching vibration of Fe_3O_4 nanoparticles is shifted from 1633 to 1645 cm^{-1} and this may be due to the binding of phenanthrimidazole with the superparamagnetic nanoparticles and the binding interaction is shown in Figure 8.

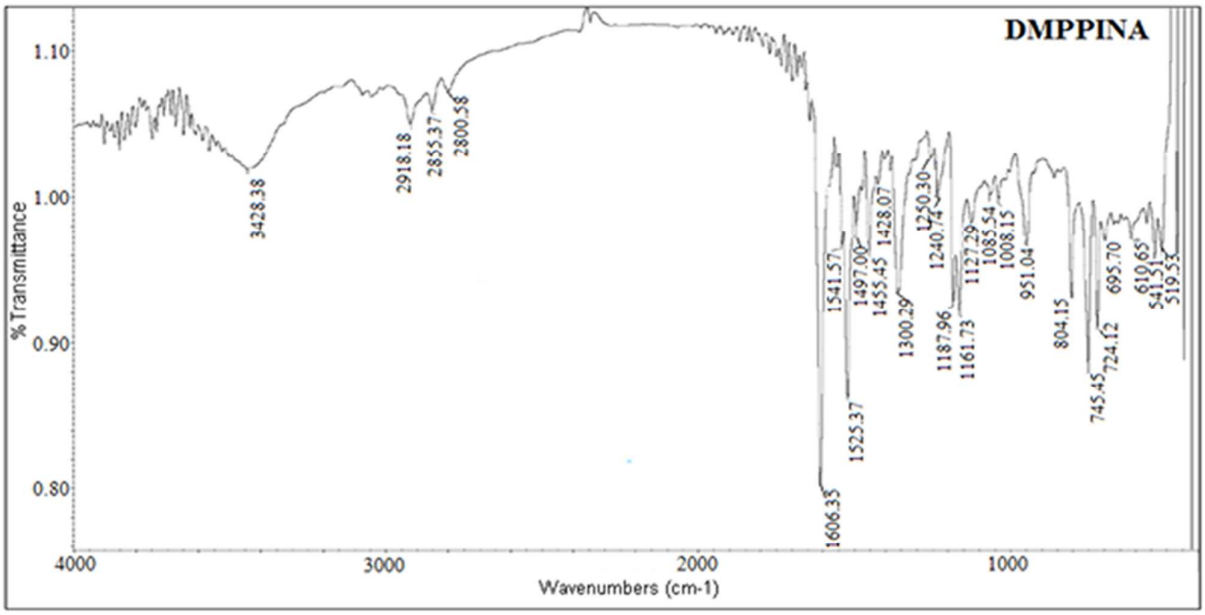

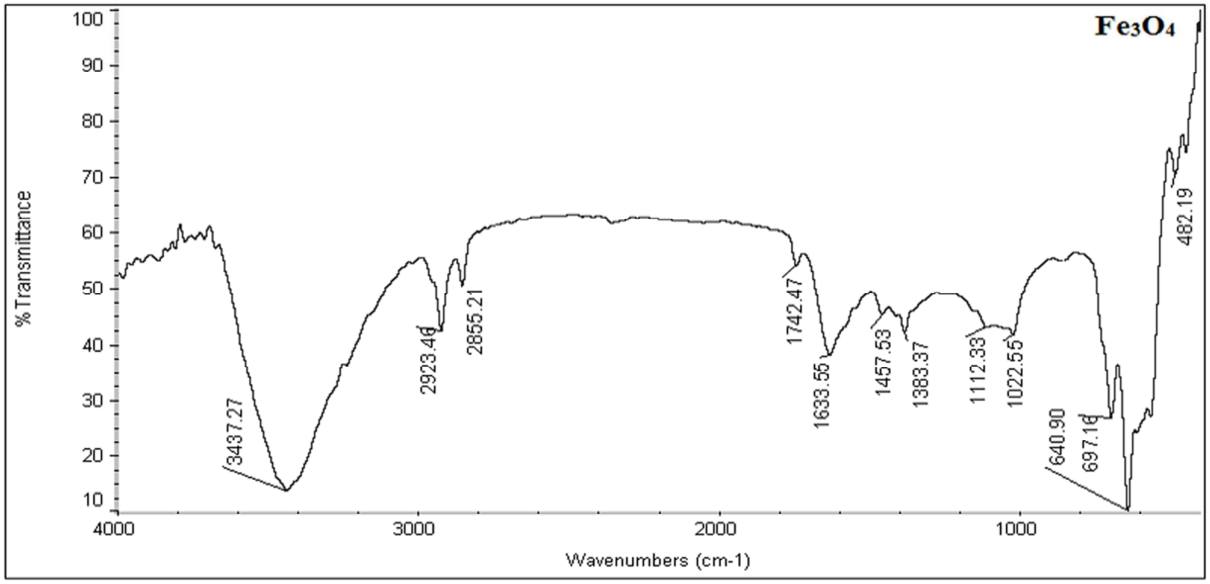

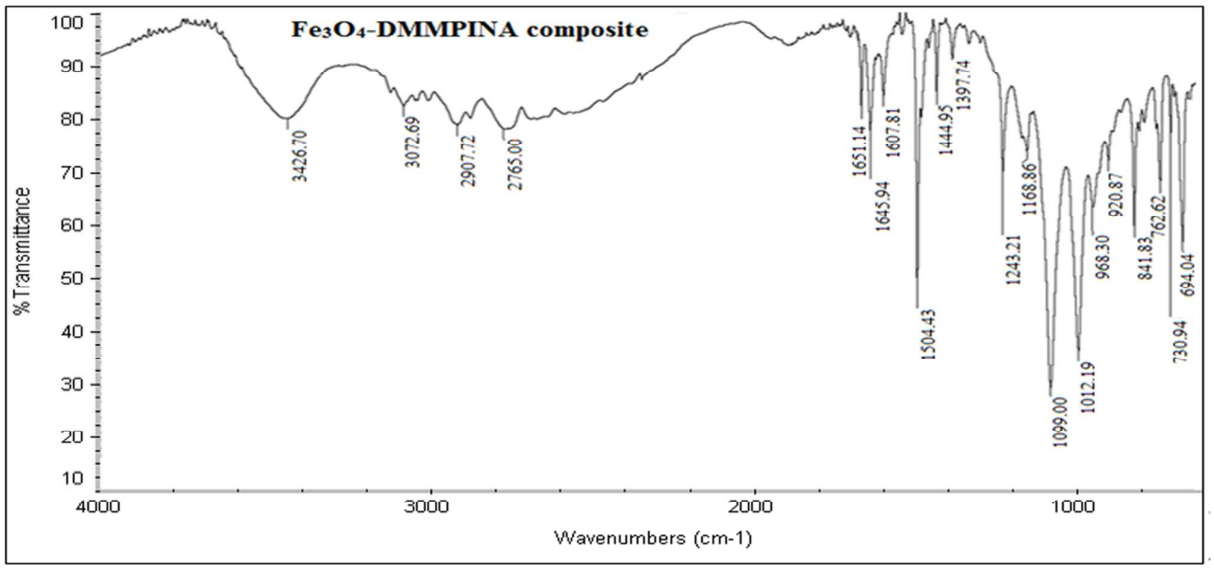

Figure 7. Fourier transform infrared spectra of (**a**) DMPPINA; (**b**) cubic Fe_3O_4 nanoparticles; (**c**) Fe_3O_4-DMPPINA composite

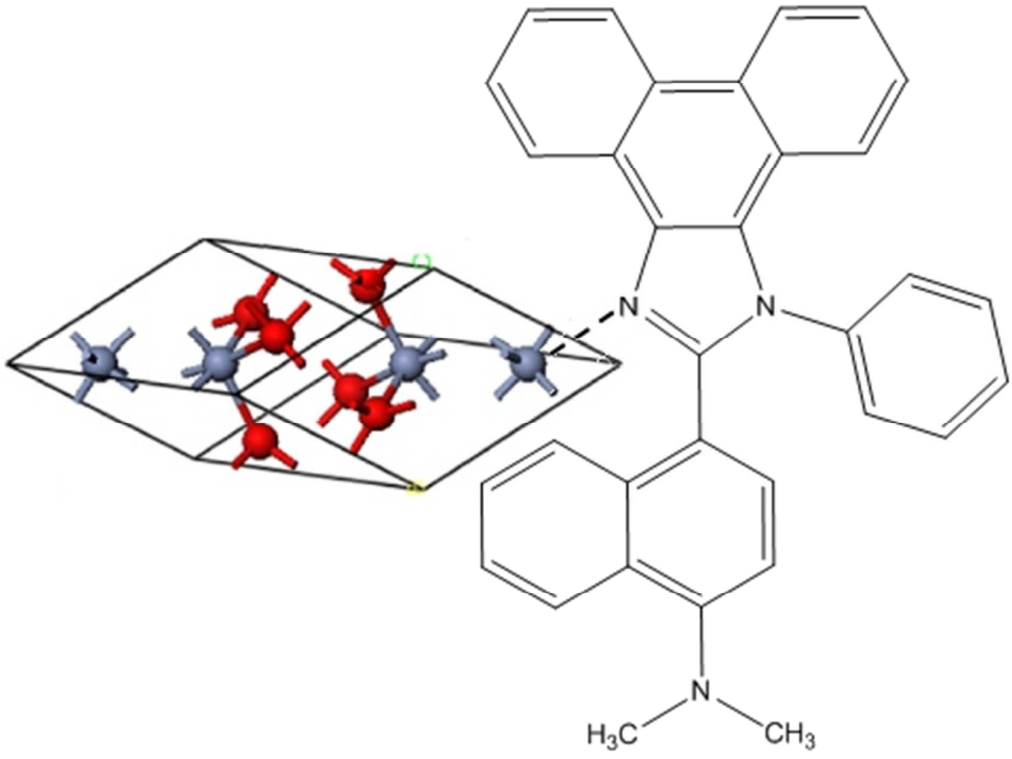

Figure 8. Attachment of phenanthrimidazole to cubic Fe_3O_4 nanoparticles

Table 2: IR data of DMPPINA, cubic Fe_3O_4 and Fe_3O_4-DMPPINA composite

Bonding	DMPPINA	cubic Fe_3O_4	Fe_3O_4-DMPPINA composite
C=N	1606	-	1651
NH-CH	3426	-	3426
Aromatic C-C Str.	1541, 1525, 1497, 1455	-	-
C-H Bending	805, 745, 724	-	841, 762
Fe – O	-	1633	1645

The optical properties of phenanthrimidazole and Fe_3O_4 – DMPPINA composite have been probed by electronic spectral studies (Figure 9). The intensities of absorption and emission increases in the following order: Fe_3O_4 - DMPPINA composite > DMPPINA. This observation shows that the interaction of phenanthrimidazole with Fe_3O_4 lowers the energy level of the valence band of Fe_3O_4 (Figure 10). A relatively small energy gap between the lowest internal charge transfer states and the locally excited states leads to increase of the contribution of π, π^* character to the wavefunction of the charge transfer states. This causes lowering of energy with respect to a pure charge transfer state resulting in red shift of the emission.

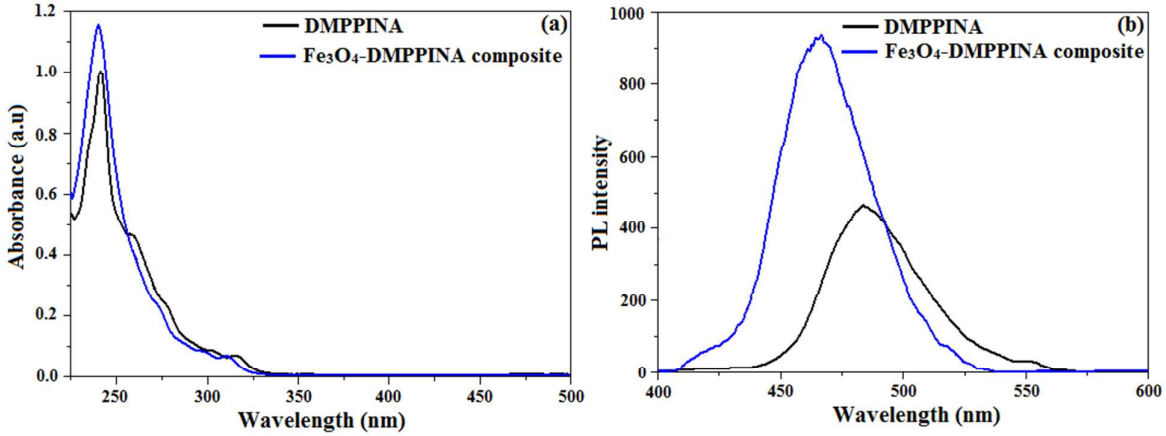

Figure 9. Absorption (**a**) and emission (**b**) spectra of DMPPINA and Fe_3O_4-DMPPINA composite

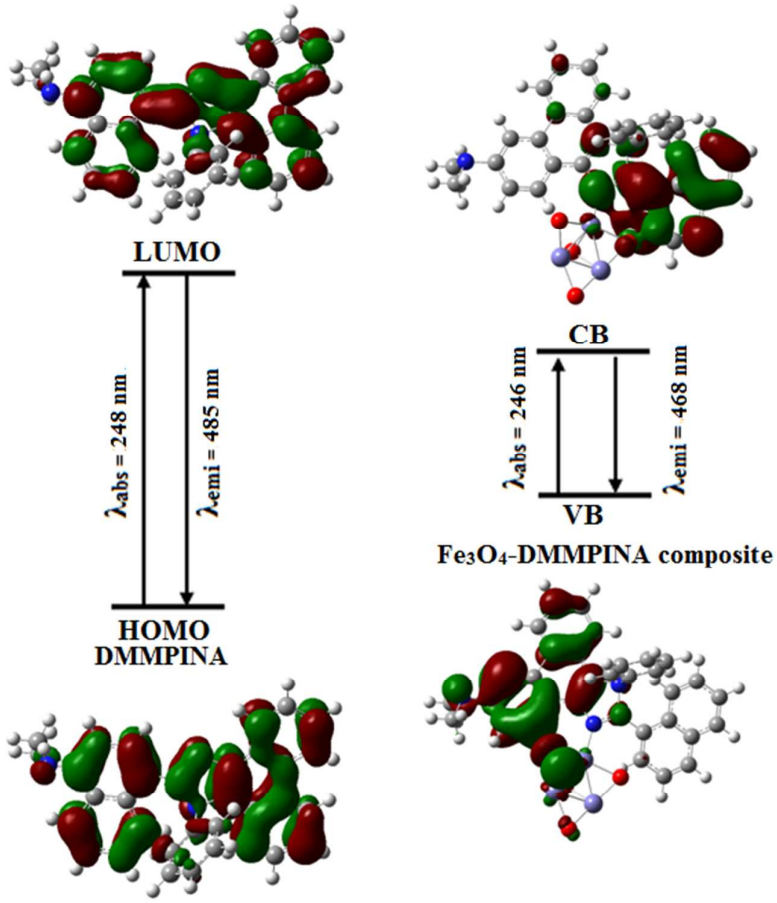

Figure 10. Energy positions of DMPPINA and Fe_3O_4-DMPPINA composite

3.4. Lifetime analysis

The fluorescence decays of phenanthrimidazole and Fe_3O_4-DMPPINA composite follow biexponential kinetics (Figure 11). The observed emission lifetime (τ) is indicative of the fact that the phenanthrimidazole interacts with nano Fe_3O_4. The determined radiative (k_r) and nonradiative (k_{nr}) rate constants are displayed in Table 3. The radiative emission of Fe_3O_4-DMPPINA composite is larger than those of DMPPINA. The life time studies reveal that the electron is transferred from the excited DMPPINA to Fe_3O_4 nanoparticles. The rate constant for electron transfer (k_{et}) can be calculated by using the equation, $k_{et} = 1/\tau_{ads} - 1/\tau$ and the calculated k_{et} is given in Table 3. The electron transfer efficiency is obtained using the equation, $E\% = (1-\tau_{composite}/\tau_{DMPPINA}) \times 100$. The unique binding interaction of nanocrystals with organic molecules can be explained on the basis of the larger surface curvature of the

nanocrystals which reduces the steric hindrance between the surface binding molecules and provides a larger number of unsaturated dangling bonds on the nanocrystal surface. Hence it is relevant to probe the binding interaction of nano clusters with DMPPINA.

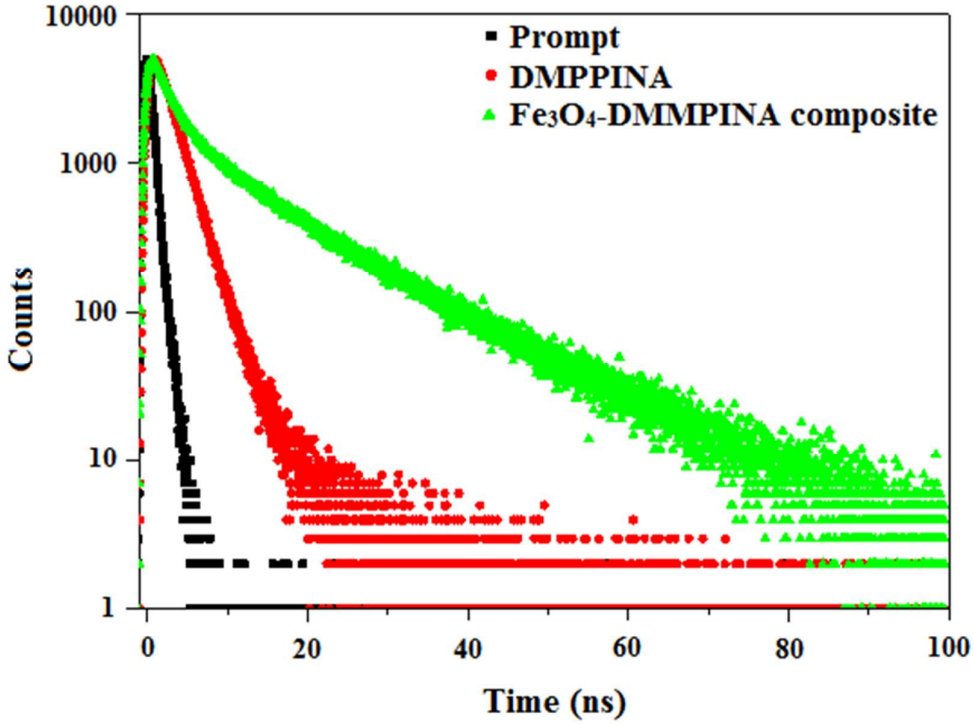

Figure 11. Life time spectra of DMPPINA and Fe_3O_4-DMPPINA composite

Table 3: Biexponential fitting parameter for fluorescence decays of DMPPINA and Fe_3O_4-DMPPINA composite

Compound	a_1 x 10^{-2}	τ_1 x 10^{-9}	a_2 x 10^{-3}	τ_2 x 10^{-9}	τ_{ave} (ns)	k_r x 10^{-8} s^{-1}	k_{nr} x 10^{-8} s^{-1}	E%	k_{et} x $10^{-10}s^{-1}$
DMPPINA	3.4621	2.0222	3.1054	3.7920	2.17	0.65	0.70	-	-
Fe_3O_4-DMPPINA	3.0422	1.9974	4.5907	1.3077	1.91	2.36	2.88	13.7	6.27

3.5. Electronic properties of iron oxide clusters and DMPPINA- Fe_3O_4 composite

In order to get a better insight on the nature of binding of the imidazole with the Fe_3O_4 surface, DFT calculations have been made with iron oxide clusters of different geometries. Fe_3O, Fe_3O_2, Fe_3O_3 and Fe_3O_4, are the clusters used for the calculation. The optimized geometries of iron oxide clusters and Fe_3O_4-DMPPINA composite are shown in Figure 12 and the optimization parameters, energy gap (E_g) and binding energies (E_b) are given in Table 4. The binding interaction between imidazole with the clusters can be analysed by binding energy, $E_b = E_{complex}-(E_{clusters} + E_{DMPPINA})$, where $E_{complex}$ is the total energy of DMPPINA adsorbed on the clusters and $E_{clusters}$ and $E_{DMPPINA}$ are the energies of the iron oxide clusters and DMPPINA, respectively. From the optimized parameters and binding energies it is confirmed that the iron atom of clusters prefer to bind through the azomethine nitrogen atom of imidazole. There is an overlap occurring between the d-orbital of iron and azomethine nitrogen atom which lead to a greater binding energy for the azomethine nitrogen site [36]. The calculated binding energy (E_b) is of the order: Fe_3O_4–DMPPINA (5.97 eV) > Fe_3O_3–DMPPINA (5.35 eV) > Fe_3O_2–DMPPINA (5.23 eV) > Fe_3O–DMPPINA (5.02 eV). This order is further supported by Fe–N bond distance. The Fe–N bond distance of Fe_3O_4–DMPPINA composite is shorter (2.03 A^0) than those of Fe_3O_3–DMPPINA (2.05 A^0), Fe_3O_2–DMPPINA (2.07 A^0) and Fe_3O–DMPPINA (2.0p9 A^0). The preferred Fe_3O_4–DMPPINA composite is most favored as compared to other composites. The covalent forces play a key role in deciding the strength of the interaction [37].

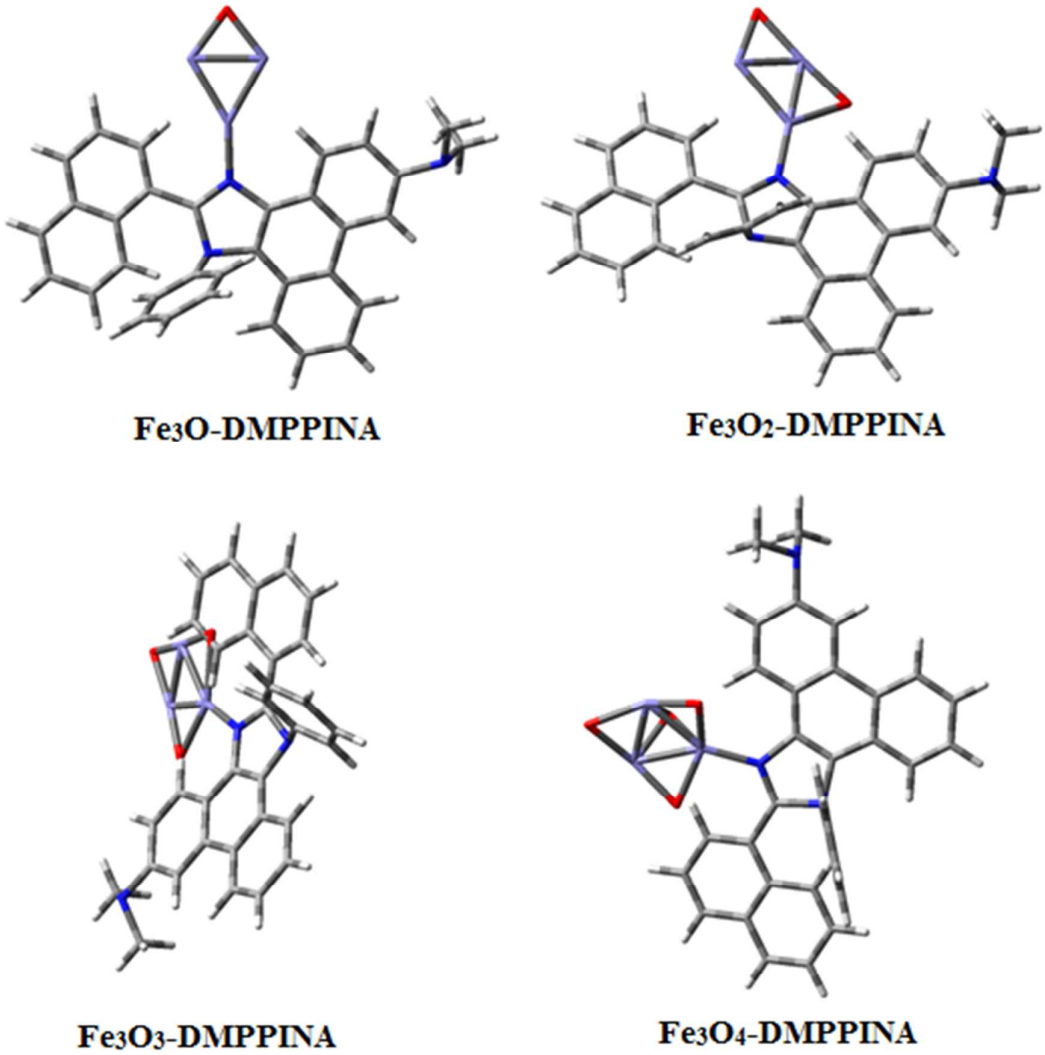

Figure 12. Optimized structures of Fe_3O–DMPPINA (**a**); Fe_3O_2–DMPPINA (**b**); Fe_3O_3–DMPPINA (**c**) and Fe_3O_4–DMPPINA (**d**) composites

In the optimized bare iron oxide clusters, the Fe–O bond length varies from 1.89 Å to 2.01 Å. Due to the adsorption of DMPPINA on iron oxide clusters, the surface structure of the Fe_3O_4 is slightly distorted. Thus the bond lengths of the composites are expanded by a smaller amount (2.03 Å, 2.09 Å). The Fe–O bond is mainly ionic in nature and charge transfer occurs from iron atom to more electronegative oxygen atom. This charge transfer is large in the surface region. To have an understanding of the extent of fractional charge transfer from imidazole to iron oxide clusters, we have shown the Mulliken charge of the

atoms of bare iron oxide clusters, imidazole and imidazole – iron oxide composites (Table S1). From the Mulliken charge analysis it is clear that there are relatively large changes in the fractional charge of the atoms which bind to the iron oxide nanomaterials and also the atoms adjacent to them. For iron oxide clusters, the oxygen atom exhibits negative charge, which are donor atoms and iron atom exhibits a positive charge, which is an acceptor atom for iron oxide clusters. All hydrogen atoms have positive charges. The iron atom exhibits a more positive charge and the azomethine nitrogen atom exhibits a more negative charge; these two atoms favor the weak interaction of Fe–N bond in imidazole – iron oxide composites. The detailed calculated values of the binding energies for imidazole with different possible attacking sites to the iron oxides are summarized in Table 4. The binding energy values suggest that the most preferred attacking site for imidazole to the iron oxide surface is azomethine nitrogen atom. The equilibrium Fe–N bond length confirms the interaction regime for covalent forces.

Table 4. HOMO and LUMO energies (eV), Energy gap (E_g, eV), Fe–N distance (A°), binding energy (E_b, eV), optimised energy (E, eV) and dipolemoments of (μ, D) of DMPPINA and composites

Compound	HOMO	LUMO	E_g	E_b		Fe–N	E	μ
				N-site	O-site			
DMPPINA	-7.04	-1.6	5.44	-	-	-	6.50	4.60
Fe_3O–DMPPINA	-4.45	-2.54	1.91	5.02	2.39	2.09	28.60	11.10
Fe_3O_2–DMPPINA	-5.28	-3.48	1.80	5.23	2.43	2.07	30.08	15.21
Fe_3O_3–DMPPINA	-7.1	-2.66	4.44	5.35	2.56	2.05	15.57	17.82
Fe_3O_4–DMPPINA	-7.25	-1.02	6.23	5.97	2.79	2.03	42.10	22.04

Energy gap (E_g) of DMPPINA, Fe_3O–DMPPINA, Fe_3O_2–DMPPINA, Fe_3O_3–DMPPINA and Fe_3O_4–DMPPINA are 5.44, 1.91, 1.80, 4.44 and 6.23, respectively (Figure S1). A large HOMO–LUMO energy gap implies higher stability and lower chemical reactivity and vice versa [38]. This shows that binding of imidazole on iron oxide cluster induces some changes in the electronic properties and the E_g values are decreased when compared with both bare imidazole and iron oxide clusters. The HOMO–LUMO analysis explains the charge transfer taking place within the imidazole–iron oxide composites. Figure S2 shows the HOMO–LUMO electron distribution plots for DMPPINA and the composites [39]. The lower energy gap shows that the charge transfer in the Fe_3O_4–DMPPINA composite is faster than the same in other composites.

3.6. Evidence for linkage

Although there are three basic sites in the phenanthrimidazole, the azomethine nitrogen is involved in the binding process with Fe_3O_4 nanoparticles. This is because of the high electron density at the azomethine nitrogen. Hence it is of interest to study the behaviour of nitrogen in acid environment. In order to prove the higher electron density at azomethine nitrogen, we have performed DFT calculation to get the molecular electrostatic potential (MEP) for the composites. The MEP map (Figure S3) shows that nitrogen atoms represent the most negative potential region (dark red). The predominance of green region in the MEP surface corresponds to a potential halfway between the two extremes red and dark blue colour.

The absorption spectra of DMPPINA at different acid concentration have been studied, trifluoroacetic acid (TFA) and H_2SO_4 have been used to maintain the acidity (Table 5). The absorption maximum (262 nm) of DMPPINA is blue-shifted to 250 nm and red-shifted to 347 nm with two isosbestic points (Figure 13) indicating the two-species (MC1 & MC2) are in equilibrium. The fluorescence maximum of DMPPINA (443 nm) at low acid concentration is blue shifted (420 nm) when excited at 250 nm and is red shifted (460 nm) on excitation at

340 nm (Figure 13). The emission at 420 nm in cyclohexane is weak and quantum yield could not be measured but it is intensive in dichloromethane (0.42) and decreases in water (0.12) whereas quantum yield at longer wavelength is maximum in cyclohexane (0.30). In order to support the experimental results (Table 6), quantum-mechanical calculations [40] were carried out for two monocations [MC1 formed by protonation of $-NMe_2$ group and MC2 obtained by the protonation of –N= atom]. The electronic spectral studies confirmed the presence of two monocations. The protonation at $-NMe_2$ group of DMPPINA induces $\pi - \pi^*$ transition which leads to a blue shift and addition of a proton at –N= atom results in a red shifted absorption due to $n - \pi^*$ transition. The fluorescence spectral analysis also supports the same conclusion. Therefore the blue shifted absorption as well as emission bands can be assigned to the MC1 monocation whereas the red shifted absorption and emission bands are assigned to the MC2 monocation.

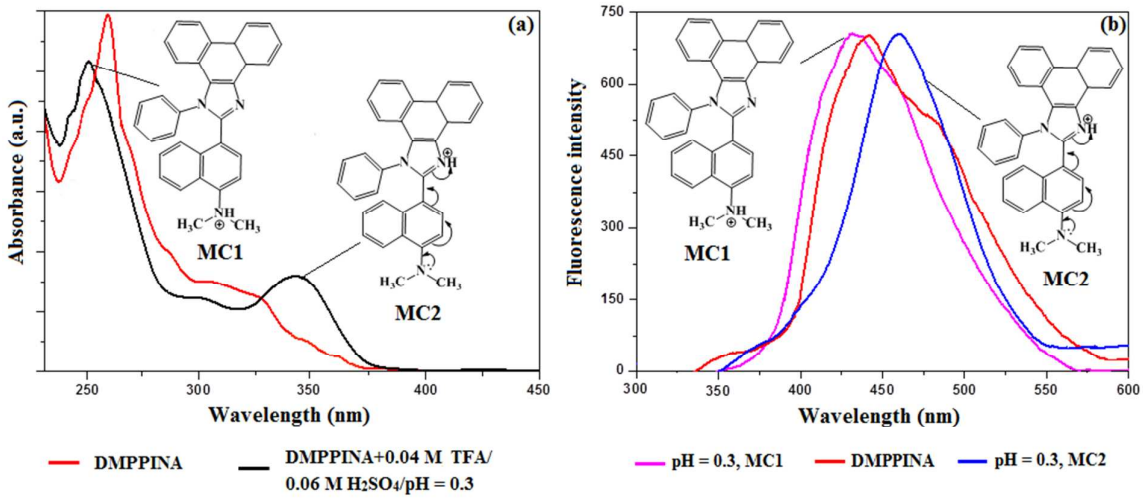

Figure 13. Absorption (**a**) and emission (**b**) spectra of the prototropic species of N,N-dimethyl-4-(1-phenyl-1H-phenanthro[9,10-d]imidazol-2-yl)naphthalen-1-amine (DMPPINA)

The dihedral angles (ϕ & θ) between the nitrogen atom and the adjacent aromatic ring (ϕ) as well as between the N,N-dimethylaminonaphthyl and phenanthrimidazole ring (θ) for DMPPINA, monocations (MC1 & MC2) are displayed in Table 6. The dihedral angle ϕ for

DMPPINA (-0.4˚), MC1 (3.8˚) and MC2 (1.8˚) are very small. The dihedral angle θ between the lone pair electrons on the $–NMe_2$ group and the naphthyl ring affect the spectral properties of the species. In MC1, the large dihedral angle (θ = 107˚) and non availability of lone pair on the $-\overset{\oplus}{N}HMe_2$ group are responsible for large blue shift [41] whereas the large red shift of MC2 relative to the DMPPINA could be attributed to the presence of the resonance structure MC2 which can be substantiated by the small dihedral θ (0.43˚) and smaller bond lengths connecting the naphthyl ring and nitrogen of the $–NMe_2$ (C–N, 1.36 A˚) and the naphthyl ring and the phenanthrimidazole moiety (C–C, 1.42 A˚) [42].

Table 5. Absorption (λ_{abs}, nm), absorbance (A), emission ($\lambda_{emi,}$ nm) and quantum yield (ϕ) of prototropic species of DMPPINA in different solvents

Species	λ_{abs}	A[a]	λ_{emi}	ϕ
Cyclohexane				
DMPPINA [0.04 M TFA]	346	1.60	390	0.54
MC1 [0.04 M TFA]	250	0.45	400	-
MC2 [0.04 M TFA]	352	1.25	441	0.30
Dichloromethane				
DMPPINA [0.0 M H_2SO_4]	282	1.50	425	0.43
MC1 [0.06 M H_2SO_4]	250	0.51	418	0.27
MC2 [0.06 M H_2SO_4]	347	0.89	491	-
Water				
DMPPINA	262	1.25	443	0.39
MC1 [pH 0.3]	250	0.68	420	0.05
MC2 [pH 0.3]	347	0.13	460	-

In non-polar solvents, MC2 is more stable than MC1 (120 kJ mol^{-1}) and the dipole moment of MC1 (13.98 D) in the ground state is very large in comparison to that of MC2

(2.72 D). Thus the proportion of a highly polar MC1 will be very small in non-polar solvents in the ground state. In polar solvents MC1 becomes more stable than MC2 by 70 kJ mol^{-1} in the ground state due to very large dipolar stabilization energy and thus its proportion in the polar solvent is increased. This explains the very small quantum yield of MC1 in non-polar solvent and MC2 in polar solvent. This is also supported by the absorbances (A) of MC1 and MC2 in cyclohexane (A_{MC1} = 0.45 & A_{MC2} = 1.25) and in water (A_{MC1} = 0.68 & A = 0.13). The decreased quantum yield of MC1 in water relative to that in dichloromethane is due to solvent induced fluorescence quenching or increase of non-radiative emission [43].

Though two monocations are formed, only one pK_a value (2.40) is obtained for the monocation − neutral molecule equilibrium which is larger than that of 2- phenylbenzoxazole (0.0) [42] and smaller than that of N,N-dimethylaniline (4.22) [44]. For 2-phenylbenoxazole, the protonation occurs at the –N= atom whereas in N,N-dimethylaniline, the protonation takes place at $–NMe_2$ group. The discrepancy can be explained as follows. From Table 6, it is clear that both $–NMe_2$ (θ = 3.78˚) and phenanthrimidazole (θ = 0.41°) moieties in DMPPINA are nearly coplanar with the naphthyl ring. Therefore the charge flow from $–NMe_2$ group to –N= atom of the heterocyclic moiety will increase, i.e. the charge density at $–NMe_2$ group will decrease and that at –N= atom will increase. This is supported by the increase of charge density at –N= atom (-0.1455) and decrease of charge density at $–NMe_2$ (-0.1996) group in neutral compared with charge density at –N= atom (-0.1294) of 2-phenylbenzoxazole and that at $–NMe_2$ (-0.2866) group of N,N-dimethylaniline. Due to this charge flow, the p*K*a value will be larger than that of 2-phenylbenzoxazole and smaller than that of N,N-dimethylaniline. The above results show that electron density at the azomethine nitrogen is higher than the rest which supports the suggested binding of azomethine nitrogen with Fe_3O_4.

Table 6. Total energy (E, au), dipole moment (μ, D), dihedral angles (ϕ˚) & (θ˚) and atomic charges P(*r*) of MC1 and MC2 and DMPPINA

Parameters	DMPPINA	MC1	MC2
ϕ	0.45	3.88	1.80
Θ	3.78	107.0	0.43
μ	4.60	13.98	2.72
E	-1530	-1917	-1544
P(*r*)N17	-0.146	0.389	0.113
P(*r*)N61	-0.120	0.192	-0.024

4. Conclusions

In summary, we report the facile synthesis of imidazole using sol-gel synthesized rutile TiO_2 nanocrystals as catalyst. The synthesized Fe_3O_4 – imidazole composite was characterized by spectral studies. The shift of Fe-O stretching vibration of from 1633 cm^{-1} to 1645 cm^{-1} confirms binding of imidazole with Fe_3O_4. The intensities of absorption, emission and conductance are higher for Fe_3O_4- imidazole composite than imidazole. The blue and red shifted absorption and fluorescence bands correspond to the two different monocations, which confirm the charge transfer from $–NMe_2$ group to azomethine nitrogen atom. We have investigated the electronic structure of imidazole interacting with different sized iron oxide clusters. The order of the binding energy for imidazole adsorbed on iron oxide clusters through the preferred azomethine nitrogen site is Fe_3O_4– imidazole > Fe_3O_3– imidazole > Fe_3O_2– imidazole > Fe_3O– imidazole and the bond distances are of the reverse order. Mulliken charge distribution shows that iron atom exhibits more positive charge and the azomethine nitrogen atom exhibits a more negative charge. Adsorption of the imidazole on iron oxide clusters modifies the electronic properties of the iron oxide clusters and the frontier molecular orbital analysis confirms the charge transfer from imidazole to iron oxide clusters.

5. Acknowledgments

One of the authors Prof. J. Jayabharathi is thankful to DST (No. SR/S1/IC-73/2010), DRDO (NRB-213/MAT/10-11), UGC (F. No. 36-21/2008 (SR)) and CSIR (NO 3732/NS-EMRII) for providing funds to this research study.

References

[1] N.S. Hush, *Coord. Chem. Rev.,* 1985, **64**, 135-157.

[2] R.A. Marcus, *J. Phys. Chem.,* 1989, **93**, 3078-3086.

[3] I.R. Gould, R.H. Young, R.E. Moody and S. Farid, *J. Phys. Chem.,* 1991, **95**, 2068-2080.

[4] I.R. Gould, D. Noukakis, L. Gomez-Jahn, R.H. Young, J.L. Goodman and S. Farid, *J. Chem. Phys.,* 1993, **176**, 439-456.

[5] J. Cortes, H. Heitele and J. Jortner, *J. Phys. Chem.,* 1994, **98**, 2527-2536.

[6] R.S. Mulliken and W.B. Person, Molecular Complexes: A Lecture and Reprint Volume, VCH, Weinheim, 1969.

[7] S.E. deLaszlo, C. Hacker, B. Li, D. Kim, M. Maccoss, N. Mantle, J.V. Pivnichny, L. Colwell, G.E. Koch, M.A. Cascieri and W.K. Hagmann, *Bioorg. Med. Chem. Lett.,* 1999, **9**, 641-646.

[8] M. Antolini, A. Bozzoli, C. Ghiron, G. Kennedy, T. Rossi and A. Ursini, *Bioorg. Med. Chem. Lett.,* 1999, **9**, 1023-1028.

[9] J. W. Black, G. J. Durant, J. C. Emmett and C. R. Ganellin, *Nature,* 1974, **248**, 65-67.

[10] Ü. Uçucu, N. G. Karaburun and İ. Işikdağ, *Il Farmaco,* 2001, **56**, 285-290.

[11] L. Wang, K.W. Woods, Q. Li, K.J. Barr, R.W. McCroskey, S.M. Hannick, L. Gherke, R.B. Credo, Y.H. Hui, K. Marsh, R. Warner, J.Y. Lee, N. Zielinski-Mozng, D. Frost, S.H. Rosenberg and H.L. Sham, *J. Med. Chem.,* 2002, **45**, 1697-1711.

[12] T. Maier, R. Schmierer, K. Bauer, H. Bieringer, H. Buerstell and B. Sachse, US Patent 4820335, *Chem. Abstr.,* 1989, **11**, 1949w.

[13] (a) S.A. Siddiqui, U. C. Narkhede, S. S. Palimkar, T. Daniel, R. J. Lahoti and K. V. Srinivasan, *Tetrahedron,* 2005, **61**, 3539-3546; (b) M. M. Heravi, M. Zakeri, N. Karimi, M. Saeedi, H. A. Oskooie and N. T. Hosieni, *Synth. Commun.,* 2010, **40**, 1998-2006.

[14] (a) J. Wang, R. Mason, D. VanDerveer, K. Feng and X.R. Bu, *J. Org. Chem.,* 2003, **68**, 5415-5418; (b) S. Sarshar, D. Siev and M.M Mjalli, *Tetrahedron Lett.,* 1996, **37**, 835-838; (c) T.F. Gallagher, G.L. Seibel, S. Kassis, J.T. Laydon, M.J. Blumenthal, J.C. Lee, D. Lee, J.C. Boehm, S.M. Fier-Thompson, J.W. Abt, M.E. Soreson, J.M. Smietana, R.F. Hall, R.S. Garigipati, P.E. Bender, K.F. Erhard, A.J. Krog, G.A. Hofmann, P.L. Sheldrake, P.C. McDonnell, S. Kumar, P.R. Young and J.L. Adams, *Bioorg. Med. Chem.,* 1997, **5**, 49-64.

[15] A. Shaabani and A. Rahmati, *J. Mol. Catal. A. Chem.,* 2006, **249**, 246-248.

[16] S. Kantevari, S.V.N. Vuppalapati, D. O. Biradar and L. Nagarapu, *J. Mol. Catal. A. Chem.,* 2007, **266**, 109-113.

[17] M. Kidwai, P. Mothsra, V. Babsal and R. Goyal, *Monatsh. Chem.,* 2006, **137**, 1189-1194.

[18] L.M. Wang, Y.H. Wang, H. Tian, Y.F. Yao, J.H. Shao and B. Liu, *J. Fluorine Chem.,* 2006, **127**, 1570-1573.

[19] G.V.M. Sharma, Y. Jyothi and P.S. Lakshmi, *Synth. Commun.,* 2006, **36**, 2991-3000.

[20] S. Balalaie and A. Arabanian, *Green Chem.,* 2000, **2**, 274-276.

[21] M. M. Heravi, K. Bakhtiari, H. A. Oskooie and S. Taheri, *J. Mol. Catal. A. Chem.,* 2007, **263**, 279-281.

[22] K. Sivakumar, A. Kathirvel and A. Lalitha, *Tetrahedron Lett.,* 2010, **51**, 3018-3021.

[23] (a) J. F. Hayes, M. B. Mitchell and C. Wicks, *Heterocycles,* 1994, **38**, 575-585; (b) L. Revesz, F. Bonne and P. Makavou, *Tetrahedron Lett.,* 1998, **39**, 5171-5174.

[24] N.J. Liverton, J.W. Butcher, C.F. Claiborne, D.A. Claremon, B.E. Libby, K.T. Nguyen, S. M. Pitzenberger, H.G. Selnick, G.R. Smith, A. Tebben, J. P. Vacca, S. L. Varga, L. Agarwal, K. Dancheck, A.J. Forsyth, D.S. Fletcher, B. Frantz, W.A. Hanlon, C.F. Harper, S.J. Hofsess, M. Kostura, J. Lin, S. Luell, E.A. O'Neill, C. J. Orevillo, M. Pang, J.

Parsons, A. Rolando, Y. Sahly, D.M. Visco and S.J. O'Keefe, *J. Med. Chem.,* 1999, **42**, 2180-2190.

[25] (a) G. Palmisano, V. Augugliaro, M. Pagliaro and L. Palmisano, *Chem. Commun.,* 2007, 3425-3437; (b) M. Mahalakshmi, B. Arabindoo, M. Palanichamy and V. Murugesan, *J. Hazard. Mater.,* 2007, **143**, 240-245; (c) M. Abu Tariq, M. Faisal and M. Muneer, *J. Hazard. Mater.,* 2005, **127**, 172-179; (d) O. S. Mohamed, A.E-A.M. Gaber and A.A. Abdel-Wahab, *J. Photochem. Photobiol. A.,* 2002, **148**, 205-210.

[26] (a) M.A. Pasha, K. Manjula and V.P. Jayashankara, *Synth. React. Inorg. Met. Org. Chem.,* 2006, **36**, 321-324; (b) S. Kumari, A. Shekhar and D.A D. Pathak, *Chem. Sci. Trans.,* 2014, **3 (2) 3 (2)**, 652-663; (c) K. V. Subba Rao, B. Srinivas, A. R. Prasad and M. Subrahmanyam, *Chem. Commun.,* 2000, 1533-1534; (d) V. Jeena and R. S. Robinson, *Beilstein J. Org. Chem.,* 2014, **10**, 1524-1535; (e) X. J. Lang, H. W. Ji, C. C. Chen, W. H. Ma and J. C. Zhao, *Angew. Chem. Int. Ed.,* 2011, **50**, 3934-3937.

[27] (a) L.A. Harris, J.D. Goff, A.Y. Carmichael, J.S. Riffle, J.J. Harburn, T.G.S. Pierre and M. Saunders, *Chem. Mater.,* 2003, **15**, 1367–1377; (b) Y.W. Chu, J.H. Hu, W.L. Yang, C.C. Wang and J.Z. Zhang, *J. Phys. Chem. B.,* 2006, **110**, 3135–3139; (c) S.O. Hwang, C.H. Kim, Y. Myung, S.H. Park, J.H. Park, J.D. Kim, C.S. Han and J.Y. Kim, *J. Phys. Chem. C.,* 2008, **112**, 13911–13916; (d) W.J. Dong, X. Li, L. Shang, Y.Y. Zheng, G. Wang and C.R. Li, *Nanotechnology,* 2009, **20**, 35601–35607.

[28] H.B. Xia, J.B. Yi, P.S. Foo and B.H. Liu, *Chem. Mater.,* 2007, **19**, 4087–4091.

[29] (a) J.P. Ge, Y.X. Hu, M. Biasini, W.P. Beyermann and Y.D. Yin, *Angew. Chem. Int. Ed.,* 2007, **46**, 4342–4345; (b) J.P. Ge, Y.X. Hu, M. Biasini, C.L. Dong, J.H. Guo, W.P. Beyermann and Y.D. Yin, *Chem. Eur. J.,* 2007, **13**, 7153–7161.

[30] (a) Z. Zhang and M.X. Wan, *Synth. Met.,* 2003, **132**, 205–212; (b) J.G. Deng, X.B. Ding and W.C. Zhang, *Polymer,* 2002, **43**, 2179–2184.

[31] (a) Q. Huang and L. Zhang, *Carbohydr. Polym.,* 2011, **83**, 1363-1369; (b) S.T. Bae, S.W. Lee and Y. Takemura, *Appl. Phys. Lett.,* 2006, **89**, 252503-252505; (c) H. Xu, N. Tong, L. Cui, Y. Lu and H. Gu, *J. Magn. Magn. Mater.,* 2007, **311**, 125-130; (d) M. Shao, L. Yan, H. Pan, I.Ivanov and Bin Hu, *Adv. Mater.,* 2011, **23**, 2216–2220; (e) H.B. Radousky and H. Liang, *Nanotechnology,* 2012, **23**, 502001-502036.

[32] (a) L. Xie, S. Ma, Q. Yang, F. Lan, Y. Wu and Z. Gu, *RSC Adv.*, 2014,**4**, 1055-1061; (b) F. Yan, J. Li, J. Zhang, F. Liu and W. Yang, *J. Nanopart. Res.,* 2009, **11**, 289-296; (c) M.A. Neouze and U. Schubert, *Monatsh. Chem.,* 2008, **139**, 183-195; (d) H. Wu, H. Zhu, J. Zhuang, S. Yang, C. Liu and Y. Charles Cao, *Angew. Chem.,* 2008, **47**, 3730–3734; (e) H. Stephanie, S.S. Andrei, L.R. Andrey, F. Jochen and S.S. Ulrich, *Curr. Nanosci.,* 2006, **2**, 135-141; (f) M.V. Kovalenko, M.I. Bodnarchuk and D.V. Talapin, *J. Am. Chem. Soc.*, 2010, **132 (43)**, 15124–15126; (g) X. Lu, M. Niu, R. Qiao and M. Gao, *J. Phys. Chem. B*, 2008, **112 (46)**, 14390–14394; (h) Q. Xiao, X. Tan, L. Ji and J. Xue, *Synth. Met.,* 2007, **157**, 784–791; (i) K.R. Reddy, K.P. Lee and A.G. Iyengar, *J. Appl. Polym. Sci.,* 2007, **104**, 4127–4134; (j) W. Yu, H. Xie, L. Chen and Y. Li, *Colloids Surf., A,* 2010, **355**, 109–113; (k) J. Deng, Y. Peng, C. He, X. Long, P. Li and A.S.C. Chan, *Polym. Int.,* 2003, **53**, 1182-1187.

[33] (a) W. H. Melhuish, *J. Phys. Chem.,* 1961, **65**, 229; (b) Gaussian 03, Revision C.02, M. J. Frisch, G. W. Trucks, H. B. Schlegel, G. E. Scuseria, M. A. Robb, J. R. Cheeseman, J. A. Montgomery, Jr., T. Vreven, K. N. Kudin, J. C. Burant, J. M. Millam, S. S. Iyengar, J. Tomasi, V. Barone, B. Mennucci, M. Cossi, G. Scalmani, N. Rega, G. A. Petersson, H. Nakatsuji, M. Hada, M. Ehara, K. Toyota, R. Fukuda, J. Hasegawa, M. Ishida, T. Nakajima, Y. Honda, O. Kitao, H. Nakai, M. Klene, X. Li, J. E. Knox, H. P. Hratchian, J. B. Cross, V. Bakken, C. Adamo, J. Jaramillo, R. Gomperts, R. E. Stratmann, O. Yazyev, A. J. Austin, R. Cammi, C. Pomelli, J. W. Ochterski, P. Y.

Ayala, K. Morokuma, G. A. Voth, P. Salvador, J. J. Dannenberg, V. G. Zakrzewski, S. Dapprich, A. D. Daniels, M. C. Strain, O. Farkas, D. K. Malick, A. D. Rabuck, K. Raghavachari, J. B. Foresman, J. V. Ortiz, Q. Cui, A. G. Baboul, S. Clifford, J. Cioslowski, B. B. Stefanov, G. Liu, A. Liashenko, P. Piskorz, I. Komaromi, R. L. Martin, D. J. Fox, T. Keith, M. A. Al-Laham, C. Y. Peng, A. Nanayakkara, M. Challacombe, P. M. W. Gill, B. Johnson, W. Chen, M. W. Wong, C. Gonzalez, and J. A. Pople, Gaussian, Inc., Wallingford CT, 2004.

[34] C. Karunakaran and P. Gomathisankar, *ACS Sustainable Chem. Eng.,* 2003, **1**, 1549-1555.

[35] C. Karunakaran, S. SakthiRaadha, P. Gomathisankar and P. Vinayagamoorthy, *Powder Technol.,* 2013, **246**, 635–642.

[36] S. Saha and P. Sarkar, *Phys. Chem. Chem. Phys.,* 2014, **16**, 15355–15366.

[37] (a) C. Arunagiri, A. Subashini, M. Saranya and P. T. Muthiah, *Ind. J. Appl. Res.,* 2013, **3**, 78–81; (b) A. V. Kachynski, A. N. Kuzmin, M. Nyk, I. Roy and P. N. Prasad, *J. Phys. Chem. C.,* 2008, **112**, 10721–10724.

[38] (a) P.K. Chattaraj and B. Maiti, *J. Am. Chem. Soc.,* 2003, **125**, 2705–2710; (b) P.G. Parr and R.G. Pearson, *J. Am. Chem. Soc.,* 1983, **105**, 7512–7516.

[39] B. Wang, S. Nagase, J. Zhao and G. Wang, *J. Phys. Chem. C.,* 2007, **111**, 4956–4963.

[40] B.M. Wepster, in: W. Klyne, P.D.B. dela Mare Eds., Progress in Stereochemistry, Academic Press, New York, 1958, **vol. 2**, ch. 4.

[41] J.K. Dey and S.K. Dogra, *Ind. J. Chem.,* 1990, **29A**, 1153.

[42] (a) J.K. Dey and S.K. Dogra, *J. Phys. Chem.,* 1994, **98**, 3638-3644; (b) J.K. Dey and S.K. Dogra, *Bull. Chem. Soc. Jpn.,* 1991, **64**, 3142-3152. (c) S.K. Dogra, *Proc. Indian Acad. Sci.,* 1992, **104**, 635-647.

[43] J.F. Ireland and P.A.H. Wyatt, *Adv. Phys. Org. Chem.,* 1976, **12**, 131-160.

[44] G. Baddelay, J. Chadwick and H.T. Taylor, *J. Chem. Soc.,* 1956, **10**, 451-462.